

Laser assisted chemical vapor deposition synthesis of carbon nanotubes and their characterization

S.N. Bondi^a, W.J. Lackey^{a,*}, R.W. Johnson^a, X. Wang^b, Z.L. Wang^b

^a *George W. Woodruff School of Mechanical Engineering, Georgia Institute of Technology, Atlanta, GA 30332-0405, United States*

^b *School of Materials Science and Engineering, Georgia Institute of Technology, Atlanta, GA 30332-0245, United States*

Received 19 August 2004; accepted 19 November 2005

Available online 20 January 2006

Abstract

The deposition of carbon nanotubes using the laser assisted chemical vapor deposition process was studied to determine the effects of processing conditions on the quantity and quality of the tubes. A structured experimental design was utilized to test the effects of laser power, and concentration of the two precursors, acetylene and iron pentacarbonyl. Processing conditions were optimized with the assistance of heat and mass transport modeling. The synthesis of lines of carbon nanotubes as well as deposits formed under the influence of an electric field were also investigated.

© 2005 Elsevier Ltd. All rights reserved.

Keywords: Carbon nanotubes; Chemical vapor deposition; Laser irradiation; Modeling

1. Introduction

Among the most significant findings in the field of material science in the past two decades has been the advancement of research in the area of nanomaterials, more specifically those made of carbon. The carbon nanotube, which is best visualized as a planar sheet of carbon atoms (graphene) wrapped into a tube, falls into a relatively new class of carbon nanomaterials known as fullerenes. The discovery of the carbon nanotube is somewhat controversial. Most attribute the discovery to the work of Iijima in the early 1990s [1–3]. However, Tibbetts fabricated carbon nanotubes as early as the mid 1980s and speculated about the growth mechanism [4]. The material possesses unusual and extraordinary mechanical, electrical, and thermal properties and already has potential to replace several existing technologies. These applications range from use in new high strength composites to use in advanced electron-

ics applications as transistors, field emitters, and sensors [5–11].

The potential applications have driven a large thrust of research to determine a suitable manufacturing process. To date, carbon nanotubes have been synthesized in relatively small quantities. The majority of high quality carbon nanotubes have been prepared using either the electric arc discharge or laser ablation methods [12–15]. These methods of synthesis do not allow for direct deposition onto various substrate materials and are therefore unsuitable for many applications which require quantities of directly deposited material. Additionally, work has also been performed in the field of chemical vapor deposition (CVD) [16,17]. This process, commonly utilized for the manufacture of ceramics and metals, is easily scaled to commercial production levels and allows for direct deposition onto a variety of substrate materials. Laser chemical vapor deposition, or LCVD, is a derivative of CVD whereby the global heat source for the furnace is replaced with a localized spot heated by a laser. There are two types of laser CVD, pyrolytic and photolytic [18]. For pyrolytic laser CVD, the type of interest here, the chemical and physical phenomena that lead to deposition are similar to those of conventional

* Corresponding author. Tel.: +1 40489 40573; fax: +1 40489 49342.
E-mail address: jack.lackey@me.gatech.edu (W.J. Lackey).

CVD. That is, the transfer of thermal energy to the reagent from the spot heated by the laser is responsible for dissociation of the reagent molecules and the deposition process [18]. Laser CVD differs from conventional CVD in that the area of growth can be limited to that of where the laser beam passes. It maintains the capability however of being able to deposit most materials that conventional CVD is capable of, on a variety of substrates. There is very little documented work in using the LCVD process to deposit carbon nanotubes. The joint publications of Rohmund et al. and Alexandrescu et al. demonstrated that LCVD deposition of carbon nanotubes was feasible, but did not address a formal processing parameter study or the use of the laser to scan patterns of the deposit [19,20].

The mechanism, or mechanisms, by which carbon nanotubes form is not without controversy [7]. For the catalyzed substrate process, nanometer size metal particles such as nickel, iron, or other metals are thought to promote fiber and tube growth. Growth can occur either below or above the catalyzed particle as carbon is precipitated from the particle which has become supersaturated with carbon.

For use in applications, it has been shown that the orientation of nanotubes on their prospective substrates is very important, particularly for their use in field emitters. Several other studies have shown success in using electric fields to control the orientation of carbon nanotubes during synthesis between horizontal electrodes [21–23]. These have also included the effects of different biases applied to the substrate [24]. These experiments showed that the electric field had a significant effect on the directionality of growth. Also of importance to mention is that others have achieved orient growth without mention of an electric field or special substrate preparation [20]. This is curious as the LCVD formed nanotubes presented here did not align themselves under standard growth conditions and is the primary reason for the study of the electric field interaction with nanotube growth.

The primary objective of this research was to identify and quantify the relationships between the key laser CVD process parameters of laser power, reagent type, reagent concentration, and pressure with the quantity and quality of carbon nanotubes synthesized. It was also desired to demonstrate that laser CVD could be used to fabricate lines of tubes and to control the orientation of the tubes by use of an electric field, since these features are required for some applications such as field emitters. Thermal modeling was used to assist achieving these objectives.

2. Experimental

The design of the LCVD system used is shown in Fig. 1, and described in further detail elsewhere [25–28]. In brief, the system is designed around a 100 W carbon dioxide laser which operates at a wavelength of 10.6 μm , which can be focused to a spot diameter between 3.9 mm and 0.2 mm allowing for flexibility in the size of the area where deposition occurs. This is the only source of heating used in the

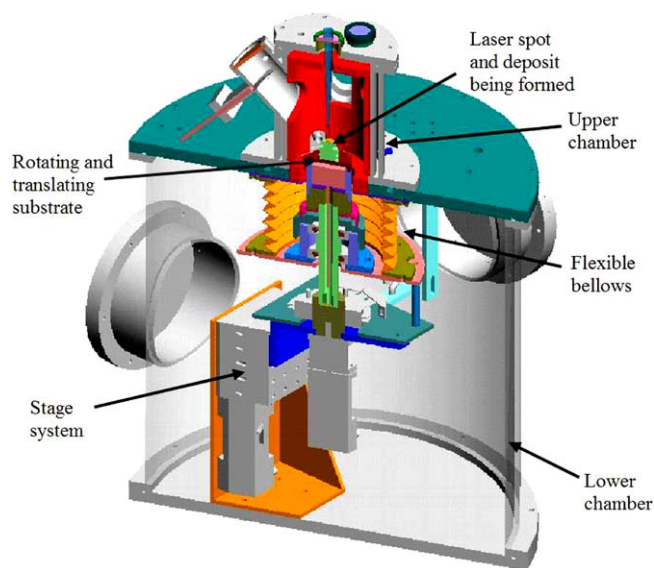


Fig. 1. Cross-sectional view of the laser CVD reactor.

experiments described here. The system housing is comprised of two chambers, an upper one which can be either statically filled or operated under constant flow of reagents, and a bottom chamber which houses moveable stages. The two chambers are separated by means of a flexible bellows, to prevent potentially corrosive reagents and reaction by products from affecting equipment below. The reactor operates with a stationary beam and optics. A substrate holder, is attached to three linear and one rotational stages housed in the lower chamber, providing a total of four degrees of freedom. The seals and the vacuum system in use allow for an operable range between pressures of 50 and 1000 Torr, however prior work has demonstrated that minimum contamination occurs at the lower range of that scale for this particular system.

The main method for nanotube synthesis involved the use of the floating catalyst method, whereby a mixture of iron pentacarbonyl, acetylene, and argon reagents was used. The iron pentacarbonyl reagent, which is liquid at standard conditions, was delivered to the upper chamber by means of a vaporizer and carrier gas consisting of acetylene, argon, or a mixture of the two. The system has an available reagent delivery nozzle, which can be used in experiments with constant reagent flow. However, the experiments described here used a static fill with no flow during the experiment. This was possible because the large volume of the upper chamber (approximately 3 L) ensured that the reagents would not be consumed during the relatively short experiments (on the order of a few minutes). Additionally, work with the reagent delivery nozzle on this system has been shown to blow poorly adhered deposit off of the substrate.

The system is equipped with a thermal imaging camera that links back to a control algorithm to adjust the power of the laser, if constant temperature is desired. The lower detectable temperature limit for this system is approxi-

mately 1200 K and is thus above the deposition temperatures used to form carbon nanotubes. In light of this, all experiments utilized a constant power scheme. Other variables that can influence the substrate temperature, given a certain laser power, were all held constant to effectively eliminate variations between samples; these included but are not limited to substrate size and surface preparation. The system has successfully deposited carbon nanotubes using several different substrate materials, including silicon, graphite, and grafoil. The experimental designs here focused on the use of graphite because the properties of the prepared substrates were most compatible with the system. Additional work has been done to demonstrate that deposition on other materials is possible.

The electric field generator used in some experiments is shown in Fig. 2. The majority of the device, was machined out of Macor, a machinable ceramic. The top electrode consisted of a tungsten screen, chosen for its high melting temperature. The lower electrode was fabricated out of Inconel. The entire device was placed on top of the substrate holder in the top reaction chamber, with the substrate placed on the lower plate in the device. Care was taken to ensure that the device was made thick enough to prevent arcing to the rest of the chamber, particularly the substrate holder. The graphite holder was mounted to a shaft which directly connected to the stage subsystem in the lower chamber. The Macor prevented arcing to the stage and chamber which could potentially damage the LCVD system. For this reason, nylon screws were also used. The electrical contacts were connected via the screws to make the bottom plate negatively biased and the top screen positive. The field generator was powered by a high voltage (2500 V), low current (40 mA) power supply that was connected to a standard electrical outlet.



Fig. 2. The electric field generator used in experimentation.

2.1. Codeposited carbon nanotube processing study

We and others have deposited carbon nanotubes using three LCVD approaches [28]. These are deposition onto a pre-catalyzed substrate, sequential LCVD of the catalyst and tubes, and codeposition, i.e., simultaneous deposition of the catalyst and tubes. In this paper we have chosen to emphasize the codeposition process since it is likely the more technological process because of its simplicity and advantages for producing lines and arrays of nanotubes. While the nucleation and growth mechanisms for the codeposition process are certainly not fully understood, one can assume that iron deposits form as small particles on the substrate either directly or via atom migration to form particles. The iron particles then dissolve carbon which is subsequently precipitated to facilitate growth of the carbon nanotubes. We saw no evidence of homogeneous nucleation so presumably the iron deposits on the substrate rather than in the gas phase.

Carbon nanotube deposits were formed using codeposition from a combination of $\text{Fe}(\text{CO})_5$ and C_2H_2 precursors with an Ar diluent. Previous deposits, characterized using scanning electron microscopy, have shown a strong link of deposit characteristics to that of the laser power and reagent concentrations used in the reaction, with other processing variables such as pressure and deposition time playing a lesser role [28]. As such, laser power and reagent concentrations were the focus of this study. A central composite with star design was chosen involving 16 runs, with the chosen range for the three variables shown in Table 1. This is a common statistical design having the attributes of efficiently exploring the variable space and being able to identify and quantify main and interaction effects [29]. All samples were deposited at a pressure of 150 Torr, over the course of 5 min with a 3.9 mm diameter laser spot. The substrates utilized were derived from a 7.94 mm (5/16 in.) diameter rod of Poco grade ACF10Q graphite; cut into 1 mm thick slices with a diamond saw. Following cutting, substrates were polished to allow for an even surface for deposition. Additionally, the substrates were also baked in an air oven at 65 °C in the presence of a desiccant for several hours before use to insure dryness.

Samples were characterized using SEM and TEM techniques. SEM analysis was performed on as-deposited samples to determine the quantity of nanotubes grown, in addition to their size and location with respect to the laser spot. For each sample, the region of the substrate of densest growth was established and used for further analysis.

Table 1
Processing variable limits for experimental design

Limits	Variables		
	Laser power (W)	$\text{Fe}(\text{CO})_5$ concentration (%)	C_2H_2 concentration (%)
Low	40.0	0.65	0.65
High	90.0	4.85	4.85

The quantity of carbon nanotubes grown was determined on a relative basis to the other samples produced. Scores were established based on a scale of 1–5, with five being the densest growth. The diameters of the nanotubes in this region were also measured using an online measuring tool in the SEM. Further analysis was performed using a TEM to unequivocally establish if tubes or fibers were produced.

3. Thermal modeling

Previous experiments have demonstrated that temperature and temperature gradient play a crucial role in nanotube deposition using LCVD [28]. As mentioned, the system normally relies on a thermal imaging system to measure and control laser output to match that of the desired reaction temperature, however the imaging system operates above the temperature region in which carbon nanotubes are grown by LCVD. Additionally, the small scale of the reaction zone has been shown to make online measurements unfeasible for the purpose of understanding what occurs thermally within the spot heated by the laser. Thus, heat and mass transport modeling were used for the purpose of describing thermally what theoretically occurs during the reaction.

Computational fluid dynamics and finite difference modeling were used to model the heat transport and convective fluid flow in and around the reaction zone. Modes of heat transfer incorporated in the model include conduction, convection, and radiative heating due to the laser beam, in and around the reaction zone. The simulation of heating was accomplished through the use of heat generation in the first layer of cells in the model. The laser profile was simulated to be Gaussian. Temperature dependant material properties were also used for both those of the substrate and the reagent gases. The models are designed primarily to determine the temperatures in and around the reaction zones for different laser powers, spot sizes, as well as substrate materials. FLUENT, a professional CFD package, was used as the solver for these efforts. Two similar models were developed; the first was designed in three dimensions and its goal was to model the heated area in three dimensions when the beam was stationary as well as to have the capability to model a scanning laser beam. A two dimensional model was also developed to compute, with much better spatial resolution, the laser heating effects in and near the laser beam for smaller diameter spots. The models were all verified against a set of experimental substrate temperature data acquired using the systems thermal imaging camera, albeit for high temperatures within the range detectable by the thermal imaging camera. The data compared favorably. The resulting models were used to help establish processing parameters for the study described in this paper.

Fig. 3 shows the geometry and boundary conditions used in the three dimensional model. This model permits the calculation of the temperature of the substrate surface as a function of radial distance from the center of the spot

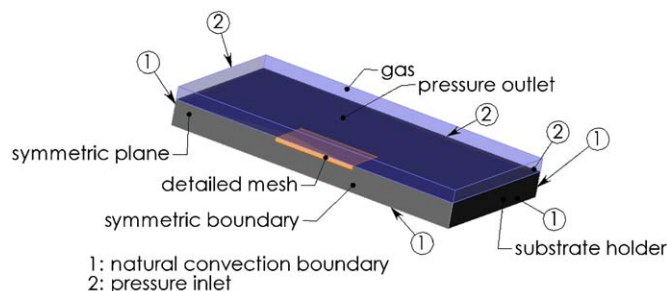


Fig. 3. Boundary conditions specified for the three dimensional model.

heated by the laser. The pressure outlet and inlet conditions are essentially open flow conditions, with no induced pressure gradient applied. The values for natural convection chosen for the sides and bottom of the substrate holder were taken to be 50 and 8 W/m² K, respectively [27]. The inputs to the model consist of the reagent gas composition and pressure, the substrate material and its material properties, as well as the laser power and beam spot diameter. The two dimensional model differed from that of the three dimensional one in that only half of the geometry shown in Fig. 3 was utilized. The input data remained the same.

3.1. Three dimensional model

The ultimate goal of the three dimensional model was to provide insight into the thermal effects of scanning a laser beam as opposed to heating a spot in a stationary manner. Traditionally, the growth of new materials via this LCVD reactor is started with the deposition of a spot of material, and only after those processing conditions are found is an attempt made to transition to a linear or layered deposit. This transition to a moving laser beam normally requires an increase in laser power to maintain the desired deposition temperature, the increase typically determined through trial and error. The end result of the three dimensional heat and mass transport model was to determine the relationship between laser spot peak temperature and scan speed. Additionally, it was desirable to learn the effect of scanning on the substrate temperature profile across the region heated by the laser.

The moving laser spot was simulated by applying the laser heating source to different cells as a function of time. FLUENT allows for easy access to the time related functions through its user defined functions. To ensure that different scan speeds would be easily comparable, a decision was made to have the laser traverse a set distance which fell within the tightly meshed region of geometry. As a result, the amount of time that each model calculation would take was different; to complete the comparison a stationary beam was also included in the set. Typical scan speeds for LCVD deposits are very slow in comparison to other laser heated processes; as such the slowest speed represented the typical scan rate (0.042 mm/s) for good multilay-

ered growth. The other speeds chosen were multiples of 3, 10, and 30 times this velocity. The laser beam diameter in all of the following simulations was chosen to be 1 mm.

The model showed some interesting yet not surprising results. Fig. 4a shows how the substrate surface temperature varies with distance from the center of the laser spot for different heating times when the laser beam is stationary. Fig. 4b and c show substrate surface temperature profiles in the direction of scanning as a function of distance from the center of the laser spot for two scanning speeds. Overall, for a scanning beam, it was found that the time scale of conduction, which is the primary mechanism for heat transport away from the beam spot, was faster than that of the scanning velocity. The results, as shown in Fig. 4, demonstrated this in that the peak temperature of the laser spot was shown to be solely a function of time for this range of scan speeds. The plot of maximum temperature versus time in Fig. 4d shows that all of the peak temperatures are essentially equivalent. The different length of the lines in the last graph is a result of a different number of time steps to complete the distance traveled. The models were run with a minimum of 60 incremental time steps, as such only a few of the time steps are shown for each case. The final time step in each case would put the laser beam at a distance from the origin of about 8.5 mm. It is

noteworthy to point out that the profiles were symmetric with respect to the beam center, i.e., the scan speeds were slow enough that conduction was significantly faster than the effect of moving the beam. The model results showed the same phenomenon in the direction perpendicular to beam travel. That is, the resulting temperature profiles were dependant only on time.

3.2. Two dimensional model

The two dimensional model was designed to be capable of accurately modeling the conditions at which experiments are run in the actual LCVD reactor. The model was designed to simulate an axisymmetric slice of the substrate holder and substrate, substantially reducing the area needing to be meshed compared to the three dimensional model previously discussed. This permitted the element size in the laser heating zone to be reduced to 0.005 mm from 0.200 mm. Consequently, laser beams with diameters as small as 0.200 mm could be effectively simulated to estimate the approximate temperatures and their distributions. Several simulations were run that matched previous experimental conditions, in terms of laser spot size, power, substrate material, reagent composition, and operating pressure.

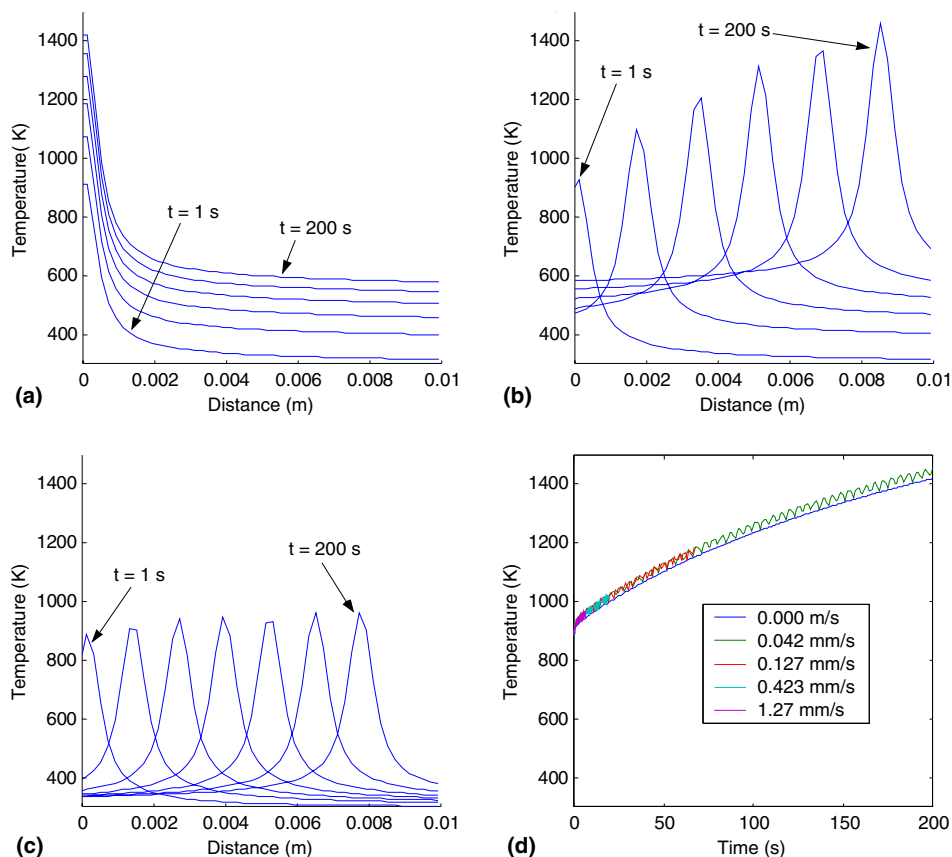


Fig. 4. Three dimensional simulation results of a scanning laser beam for various scan speeds. (a) Temperature distributions, $v = 0.000$ mm/s, (b) temperature distributions, $v = 0.042$ mm/s, (c) temperature distributions, $v = 1.270$ mm/s, (d) maximum temperature vs time step.

The simulation represented a reproduction of a set of earlier experiments whereby carbon nanotubes were synthesized utilizing a 90% argon and 10% acetylene reagent atmosphere. These experiments were performed initially using a 40 W laser spot of 3.89 mm diameter on a grafoil substrate. However, in an effort to make smaller patterns of deposits, it was desirable to be able to use a smaller diameter laser beam on other materials, while achieving the same deposit characteristics. Experimentally this has proved quite difficult even with relatively small changes in spot size. The simulation was used to predict the resulting profiles for two other materials, silicon and ATJ graphite at two laser spot sizes as well as at several levels of laser power. A sampling of the results are presented in Fig. 5. They demonstrate how the resulting temperature profile strongly depends not only on power density but also on the substrate material. The temperatures are most strongly influenced by the substrate reflectivity and thermal conductivity. These data are shown in Table 2. The broad profiles for grafoil are a result of its low conductivity through its thickness.

Table 2

Reflectivity and thermal conductivity values for simulated substrate materials

Material	Grafoil	Silicon	ATJ graphite
Reflectivity (@ $\lambda = 10.6 \mu\text{m}$)	0.50	0.23	0.00
Conductivity range (W/m K) (300–1600 K)	136–38 (planar) 5–3 (thickness)	148–22	129–45

4. Results and discussion

4.1. Processing condition study results

4.1.1. Process yield

The data collected from the SEM analysis of the samples was processed using a statistical package, Statgraphics. The results from the areas of greatest growth were analyzed using a multivariate regression at the 95% confidence level. A statistically significant correlation of the number of nanotubes grown with the concentration of acetylene (C_2H_2) and the square of the laser power was found. The resulting model, which had an R^2 value of 62%, was used

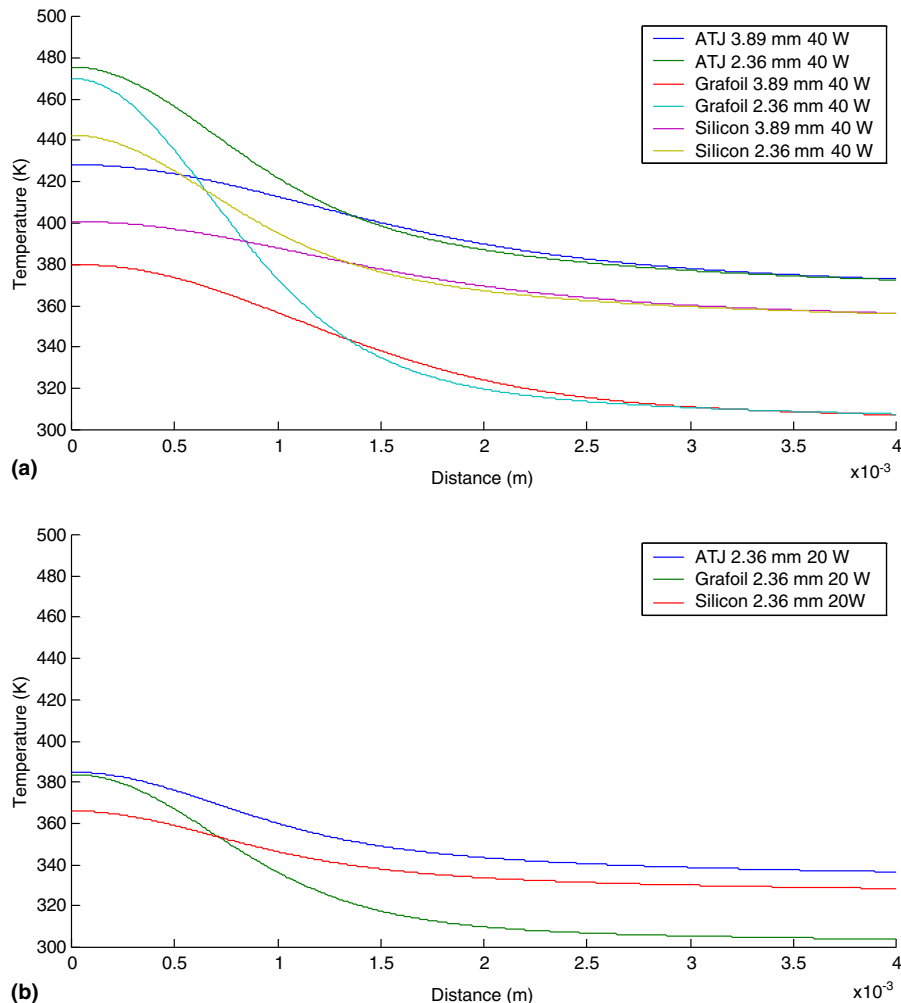


Fig. 5. Two dimensional model derived temperature profiles. (a) Temperature distributions at 40 W and (b) temperature distributions at 20 W.

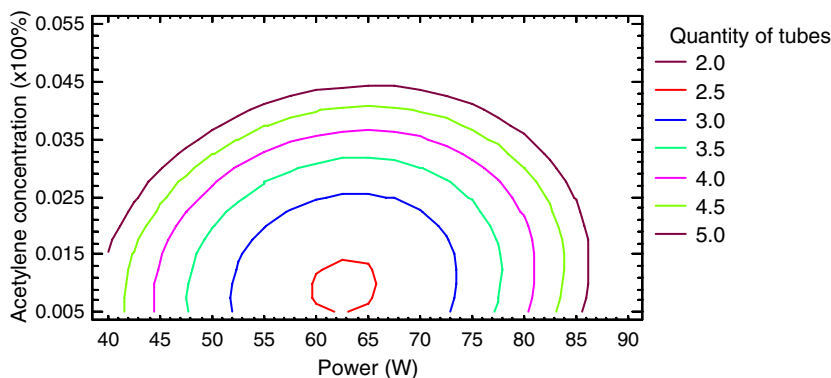


Fig. 6. Response surface showing acetylene reagent concentration and laser power effects on quantity of carbon nanotubes grown.

to establish the processing parameter map, shown in Fig. 6. This contour map shows that an increase in acetylene concentration, at moderate laser powers, will result in increased tube growth. For low laser powers and low acetylene concentrations, increasing the laser power first results in a decrease in the number of nanotubes grown. As the power is increased further, the quantity of tubes grown increases. Because of the much larger effect of acetylene concentration on the quantity of nanotubes formed than those of the other variables, a linear regression was performed to determine the extent of the correlation. The results are presented in Fig. 7. The inner and outer bands shown in Fig. 7 are the 95% confidence intervals for the linear relationship and data points, respectively. The R^2 adjusted value for the regression was 58%. In other words, 58% of the variation in the process yield could be attributed to the variation of the acetylene concentration. It is therefore reasonable to conclude that acetylene concentration has a strong influence on the quantity of nanotubes grown. It seems logical that increasing the acetylene concentration would increase the quantity of tubes grown, but the mechanism of tube growth is not sufficiently known to permit understanding of exactly why the acetylene concentration is so important. One can speculate that tube nucleation or the growth rate of tubes once nucleated is influenced

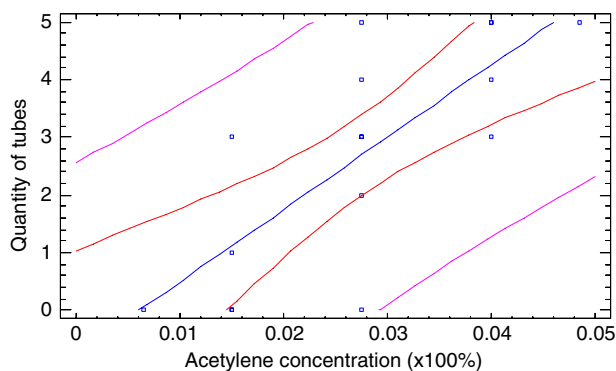


Fig. 7. Linear regression of the effect of acetylene concentration on the quantity of nanotubes grown in the region of greatest growth on the substrate.

by the local concentration of acetylene, for example, as in a first order chemical reaction such as that often observed for conventional CVD. Since not much acetylene is consumed by the growth of the small tubes, there is likely not an appreciable depletion of reagent. In other words, the local acetylene concentration may be nearly equal that of the concentration of acetylene in the input reagent mixture. There are no systematic studies in the literature against which these results can be compared.

4.1.2. Nanotube diameter

One of the objectives of this study was to determine the relationship between processing conditions and the size of the nanotubes formed. As smaller nanotubes tend to possess more useful properties, it is desirable to optimize the processing parameters such that small tubes are produced. A model was generated for tube size for the region of growth on the substrate that contained the most tubes. The measured diameters of the nanotubes were regressed against the processing conditions, and the results showed that most of the terms were statistically significant. By excluding laser power, a final model with an R^2 adjusted value of 90% was obtained. The resulting processing parameter map is shown in Fig. 8. It can be seen that overall the smallest diameter nanotubes were produced when the acetylene content was increased above that of the iron pentacarbonyl concentration. Fortunately, the high acetylene concentrations increase not only the number of tubes formed (Fig. 7) but also decreases their size, for acetylene concentrations up to about 3.5%. As the following section indicates, the contour lines in the upper left corner of Fig. 8 are likely inaccurate.

4.1.3. Validation of processing study results with experiments

The results of the processing study in terms of nanotube yield and diameter showed that a simultaneous increase in C_2H_2 and decrease in $Fe(CO)_5$ concentrations would result in a greater yield of carbon nanotubes while also decreasing their size. Several experiments were conducted to confirm this suggested trend. Samples were produced with $Fe(CO)_5$ concentrations of 0.65% and C_2H_2 concentrations of 9.70% at a laser power of 60 W. The resulting yield was

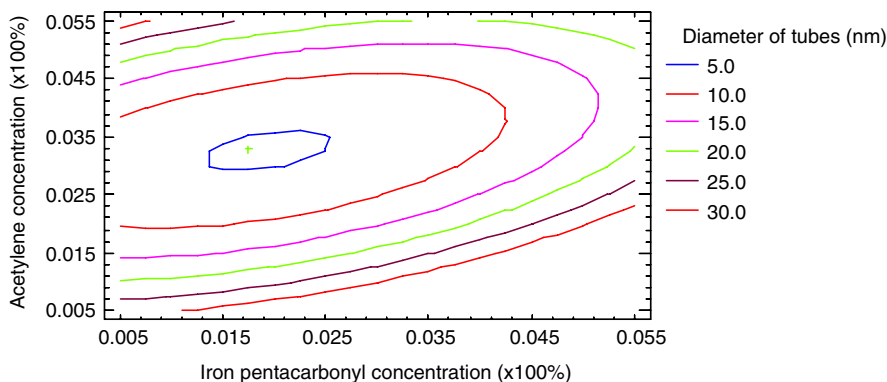


Fig. 8. Response surface of reagent concentration effects on diameter of carbon nanotubes grown.

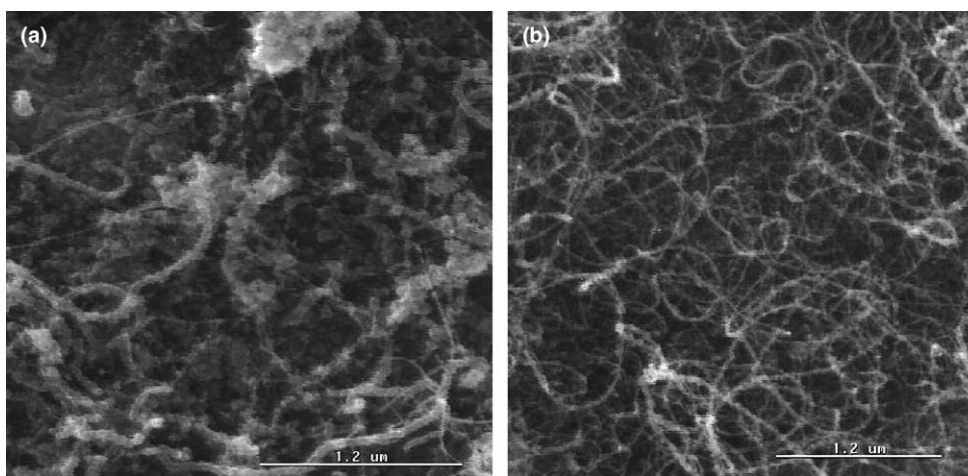


Fig. 9. Micrograph of carbon nanotubes produced using (a) non-optimized versus (b) optimized processing conditions.

impressively large and the tubes were very small, some as small as 7 nm in diameter with significant aspect ratios. The improvement could easily be seen upon analysis of many images using an SEM. As shown in Fig. 9, micrograph (a) has significantly less fine material than that of the optimized conditions (b). For comparison, the nanotubes produced in (a) were made using reagent concentrations of 4.85% $\text{Fe}(\text{CO})_5$ and 2.75% C_2H_2 . Subsequent experiments utilizing the greater C_2H_2 concentration also produced similar deposits with high yield and small sized material.

4.1.4. TEM analysis

One of the primary limitations of using SEM based characterization is that the resolution does not allow the structure of the deposit to be seen clearly. TEM analysis was therefore used to insure that the carbon nanomaterial that was produced was in fact tubular rather than solid fibers. Previous work has demonstrated that nanotubes can typically be differentiated from their solid fiber counterparts by their wall characteristics. Nanotubes synthesized using LCVD typically had walls that were smooth and uniform. In comparison to nanotube deposits, the

solid nanomaterial deposits tended to have bumpy sides, and would less often grow straight. Often, tubes and fibers could be found on the same sample, implying that they grew simultaneously. Additionally, the sizes of the carbon nanotubes grown would vary significantly. This can be seen both in the SEM micrographs presented in Fig. 9 as well as

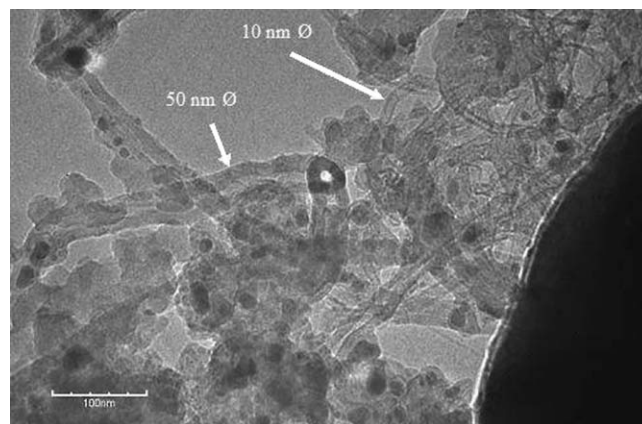


Fig. 10. TEM micrograph of clumped carbon nanomaterial showing multiple sized tubes.

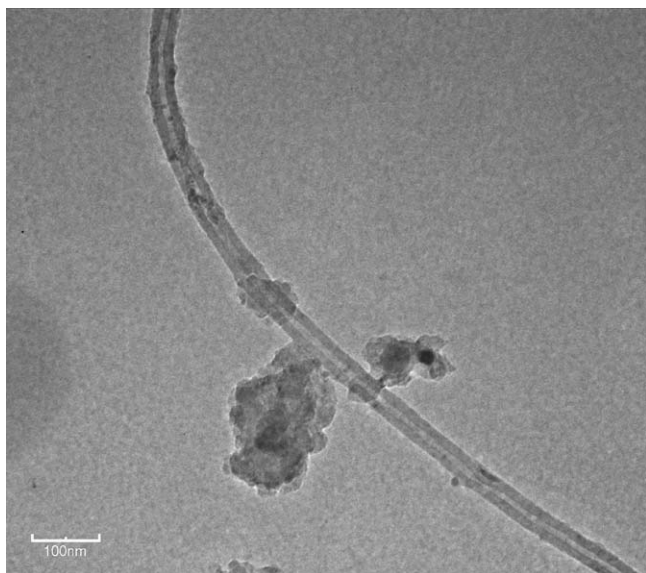


Fig. 11. TEM micrograph of a smooth walled carbon nanotube.

in the image acquired by TEM in Fig. 10. In this case the nanotubes had diameters varying between 10 and 50 nm. SEM analysis has shown evidence of nanotubes with diameters below this, with some as small as 7 nm being measured. Fig. 11 shows a typical example of what the walls of a typical LCVD produced nanotube looked like. The one pictured was taken from the sample shown in the micrograph of Fig. 9b and had a diameter of approximately 40 nm. The thickness of the walls, as well as the relatively large diameters of the nanotubes found, indicates that these nanotubes are multiwalled.

4.2. Linear carbon nanotube deposits

As previously mentioned, the LCVD system was capable of moving the substrate relative to the laser beam. This feature was utilized to generate patterns of carbon nanotubes. For these experiments the size of the laser beam was reduced to 0.2 mm which permitted the feature width of the deposit to fit on the graphite substrates. Processing conditions for these experiments followed the results of the aforementioned processing condition study. The thermal modeling discussed earlier showed that the heating process is transient, and that maximum spot temperature is highly dependant on time. Therefore it would be expected that the laser power per unit area necessary to achieve the same temperature in a moving beam would need to be significantly greater than that of a stationary beam. This was shown experimentally and the laser powers utilized for these experiments varied between 30 and 57 W. Since the diameter of the laser beam is smaller than that used in the stationary experiments, the laser power per unit area is considerably higher. A multiple pass approach was chosen to deposit the lines of material. This used a series of 20 passes at a scan speed of 2.54 cm/min to generate sufficient

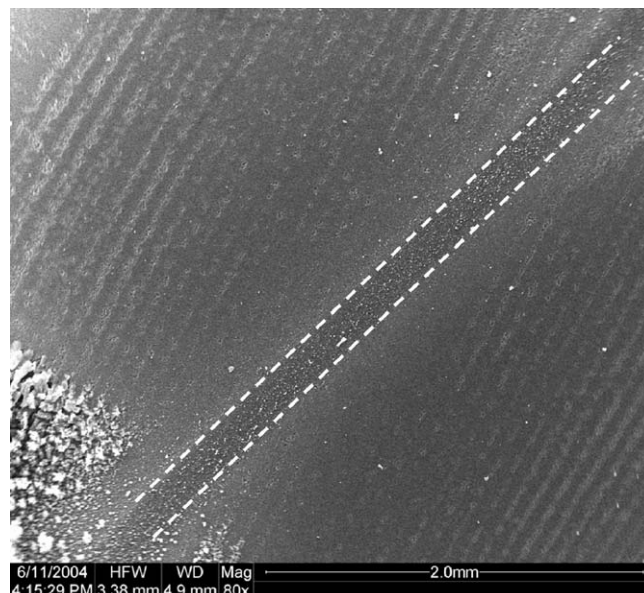


Fig. 12. Line of carbon nanomaterial. The dashed lines delineate the region of growth.

growth. Experiments showed that this method was more effective in preventing unwanted uncontrolled growth at the periphery of the laser spot in comparison to using one pass at a much slower scan speed. After synthesis, the samples were analyzed in the SEM to determine if nanotubes were produced and the width of the line of deposited material. As shown in Figs. 12 and 13, a line 0.17 mm wide containing carbon nanotubes was produced. While sufficient research was not performed to optimize the process, it is significant that formation of a line containing carbon nanotubes was shown to be feasible by laser CVD. Since the multiple pass process was used, additional

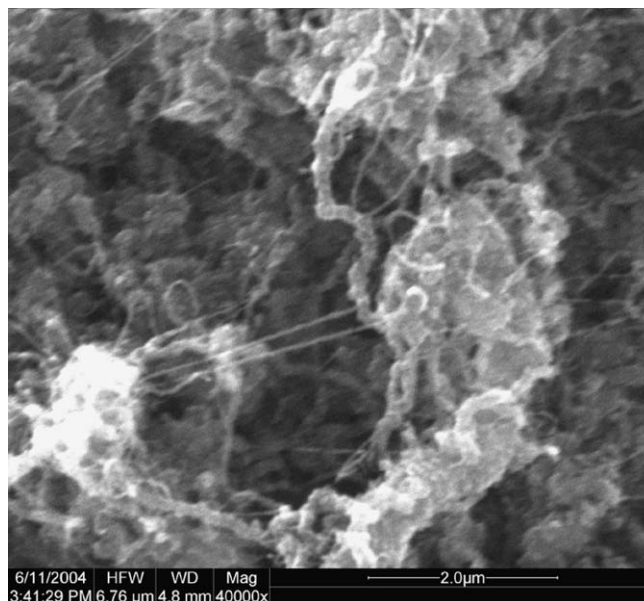


Fig. 13. Carbon nanotubes found within the line presented in Fig. 12.

research should be performed to determine how the laser beam affects tubes grown during an earlier pass.

4.3. Electric field influenced deposits

Samples were also produced with an electric field generator using the results of the previously mentioned processing conditions study. The device was designed so that an electric field could be developed perpendicular to the substrate surface. This created a field such that the nanotubes were made to ‘stand up’ on the substrate during their growth. The upper electrode consisted of a tungsten screen mesh. This screen was attached to a ceramic holder which was designed to hold a bottom electrode made from a sheet of Inconel, on which the substrate would sit. The 1.27×1.27 mm openings in the screen permitted passage of the laser beam through to the substrate. The spacing between the two electrodes was 1 cm with a maximum supplied voltage of 2000 V. In agreement with Paschen’s law, which shows that pressure and gas type influence the field strength for the onset of arcing, it was necessary to increase the operating pressure of the system during deposition to 1000 Torr and to use H_2 as a diluent instead of Ar to avoid electric discharge [30]. Arcing was undesirable since it typically resulted in an increase in the production of soot formations which would link the top and bottom electrodes, causing a current which decreased the field strength. Experiments were conducted with the same partial pressures of the $Fe(CO)_5$ and C_2H_2 reagents as those of experiments without the electric field. In addition, samples were also prepared utilizing the field generator device with the greater pressure and H_2 diluent but without the electric field to verify that growth was equivalent to that of previous experiments.

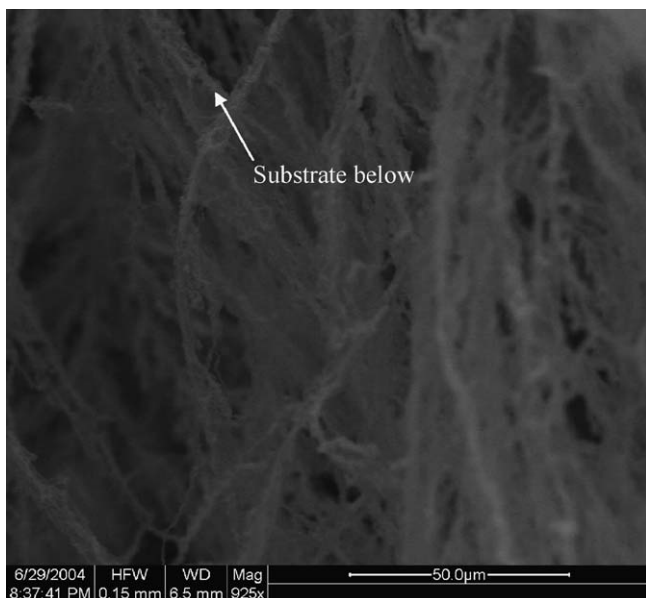


Fig. 14. Oriented carbon nanotube ropes and carbon fibers.

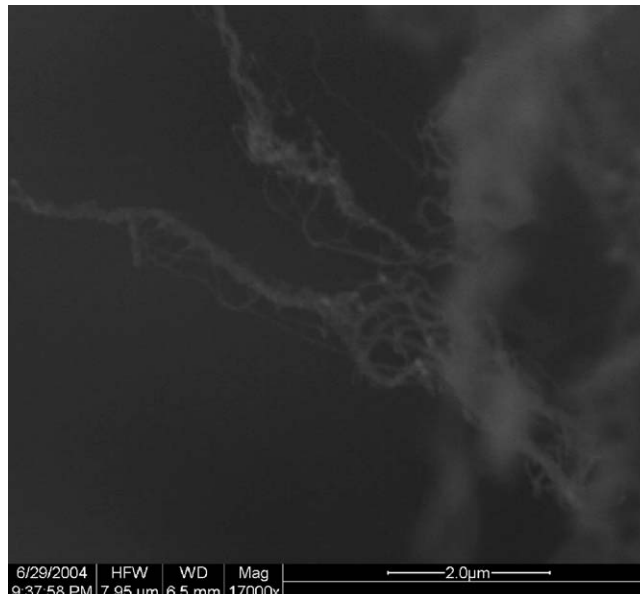


Fig. 15. Oriented carbon nanomaterial consisting of nanotubes.

All samples produced were analyzed using an SEM to determine the directionality of growth of the resulting nanotubes. The SEM analyses showed that a significant number of carbon fibers and carbon nanotube ropes were formed in the direction parallel to the electric field. These ropes are seen oriented vertically from the graphite substrate in Fig. 14, with their structure seen in better detail in the higher magnification micrograph of Fig. 15. These results suggest that oriented deposits can be made by LCVD utilizing an electric field as previously shown for CVD deposits [22–24].

5. Summary and conclusions

The work presented here demonstrates the capabilities of LCVD as a synthesis method for carbon nanotubes. The codeposition growth studies presented show that process yield can be increased by utilizing a reagent combination that has hydrocarbon levels above that of the catalyst reagent. Higher acetylene concentrations and lower iron pentacarbonyl concentrations yield more tubes and smaller tubes. The results of these studies were further used to produce lines of carbon nanotubes as well as oriented growth using an electric field. Finally, the thermal modeling presented can be used, in the absence of thermal feedback and control, to approximate the deposition temperature for different laser powers.

References

- [1] Iijima S, Ichihashi T. Single-shell carbon nanotubes of 1-nm diameter. *Nature* 1994;363:603–5.
- [2] Dresselhaus M, Dresselhaus G, Saito R. Physics of carbon nanotubes. *Carbon* 1995;33(7):883–91.
- [3] Dresselhaus M, Dresselhaus G, Eklund P, Saito R. Carbon nanotubes. *Phys World* 1998(January):33–8.

- [4] Tibbetts G. Why are carbon filaments tubular? *J Cryst Growth* 1984; 66:632–8.
- [5] Ning J, Zhang J, Pan Y, Guo J. Surfactants assisted processing of carbon nanotube-reinforced SiO₂ matrix composites. *Ceram Int* 2004; 30(1):63–7.
- [6] Cadek M, Coleman J, Barron V, Hedicke K, Blai W. Morphological and mechanical properties of carbon-nanotube-reinforced semicrystalline and amorphous polymer composites. *Appl Phys Lett* 2002; 81(27):5123–5.
- [7] de Heer W, Châtelain A, Ugarte D. A carbon nanotube field-emission electron source. *Science* 1995;270(5239):1179–80.
- [8] Choi W, Chung D, Kung J, Kim H, Jim Y, Han I, et al. Fully sealed, high-brightness carbon-nanotube field-emission display. *Appl Phys Lett* 1999;75(20):3129–31.
- [9] Chopra S, McGuire K, Gothard N, Rao A, Pham A. Selective gas detection using a carbon nanotube sensor. *Appl Phys Lett* 2003; 83(11):2280–2.
- [10] Modi A, Koratkar N, Lass E, Wel B, Ajayan P. Miniaturized gas ionization sensors using carbon nanotubes. *Nature* 2003;424(6945): 171–4.
- [11] Collins P, Avouris P. Nanotubes for electronics. *Sci Am* 2000(December):62–9.
- [12] Huczko A. Synthesis of aligned carbon nanotubes. *Appl Phys A* 2002;74(5):617–38.
- [13] Maser W, Munoz E, Benito A, Martinez M, de la Fuente G, Maniette Y. Production of high-density single-walled nanotubes material by a simple laser-ablation method. *Chem Phys Lett* 1998;292(4–6): 597–693.
- [14] Journet C, Maser W, Bernier P, Loiseau A, Lamy de la Chapelle M, Lefrant S. Large-scale production of single walled carbon nanotubes by the electric-arc technique. *Nature* 1997;388:756–8.
- [15] Thess A, Lee R, Nikolaev P, Dai H, Petit P, Robert J. Crystalline ropes of metallic carbon nanotubes. *Science* 1996;273(5274):483–7.
- [16] Pradhan D, Sharon M. Carbon nanotubes, nanofilaments and nanobeads by thermal chemical vapor deposition process. *Mater Sci Eng B* 2002;96:24–8.
- [17] Chow L, Zhou D, Hussain A, Kleckley S, Zollinger K, Schulte A, et al. Chemical vapor deposition of novel carbon materials. *Thin Solid Films* 2000;368(2):193–7.
- [18] Duty C, Jean D, Lackey WJ. Laser chemical vapor deposition: materials, modeling, and process control. *Int Mater Rev* 2001;46(6): 271–87.
- [19] Rohmund F, Morjan R, Ledoux G, Huisken F, Alexandrescu R. Carbon nanotube films grown by laser-assisted chemical vapor deposition. *J Vac Sci Technol B: Microelectron Nanometer Struct* 2002;20(3):802–11.
- [20] Alexandrescu R, Crunteanu A, Morjan R, Morjan I, Rohmund F, Falk L, et al. Synthesis of carbon nanotubes by CO₂-laser-assisted chemical vapour deposition. *Infrared Phys Technol* 2003;44:43–50.
- [21] Peng H, Ristroph T, Schurmann G, King G, Yoon J, Narayanamurti V, et al. Patterned growth of single-walled carbon nanotube arrays from a vapor-deposited Fe catalyst. *Appl Phys Lett* 2003;83(20): 4238–40.
- [22] Zhang Y, Chang A, Cao J, Wang Q, Kim W, Li Y, et al. Electric-field-directed growth of aligned single-walled carbon nanotubes. *Appl Phys Lett* 2001;79(19):3155–7.
- [23] Jang Y, Ahn J, Ju B, Lee Y. Lateral growth of aligned multiwalled carbon nanotubes under electric field. *Solid State Commun* 2003;126: 305–8.
- [24] Avigal Y, Kalish R. Growth of aligned carbon nanotubes by biasing during growth. *Appl Phys Lett* 2001;78(16):2291–3.
- [25] Lackey WJ, Rosen D, Duty CE, Jean DL, Bondi SN, Elkhatib TN, et al. Laser CVD system design operation, and modeling. *Ceram Eng Sci Proc* 2002;23(4):23–33.
- [26] Jean DL, Duty CE, Fuhrman B, Lackey WJ. Precision LCVD system design with real-time process control. In: 10th annual solid freeform fabrication symposium, UT Austin, (TX) USA, 1999, p. 59–65.
- [27] Duty CE. Design, operation, and heat and mass transfer analysis of a gas-jet laser chemical vapor deposition system. Atlanta (GA), USA, Georgia Institute of Technology, PhD thesis, 2001.
- [28] Bondi SN. LCVD synthesis of carbon nanotubes and their characterization. Atlanta (GA), USA, Georgia Institute of Technology, PhD thesis, 2004.
- [29] Wu CFJ, Hamada M. Experiments: planning, analysis, and parameter optimization. New York (NY): Wiley; 2000, p. 387–412.
- [30] Boxman R, Sanders D, Martin P. Handbook of vacuum arc science and technology: fundamentals and applications. Park Ridge (NJ): Noyes; 1995, p. 61–3.